JATIS Journal of Astronomical Telescopes, Instruments, and Systems

RESEARCH PAPER

Laser frequency comb system for the infrared Doppler instrument on the Subaru Telescope

Takuma Serizawa,[a,b,*] Takashi Kurokawa,[a,c] Yosuke Tanaka,[a,c] Jun Nishikawa,[b,c,d] Takayuki Kotani,[b,c,d] and Motohide Tamura[b,c,e]

[a]Tokyo University of Agriculture and Technology, Institute of Engineering, Tokyo, Japan
[b]National Astronomical Observatory of Japan, NINS, Tokyo, Japan
[c]Astrobiology Center, NINS, Tokyo, Japan
[d]The Graduate University for Advanced Studies (SOKENDAI), School of Science, Department of Astronomy, Tokyo, Japan
[e]University of Tokyo, Department of Astronomy, Tokyo, Japan

ABSTRACT. An exoplanet survey with a near-infrared Doppler (IRD) instrument focused on mid-to-late M-type dwarfs began in February 2019 within the framework of the Subaru Strategic Program. Because mid-to-late M-type dwarfs are brighter in the infrared region than in the visible region, a laser frequency comb (LFC) system was developed as a wavelength reference, covering the near-infrared region from 970 to 1750 nm. To stabilize the comb image on the spectrometer, the original 12.5 GHz comb generated using highly nonlinear fibers was injected into the spectrometer after optical processing, including spectral shaping, depolarization, and mode scrambling. An inline fiber module was introduced to enable any optical system configuration for the optical processor. This fiber-optic configuration in the LFC system allows for long-term stability and easy repair. Moreover, simple remote control of the LFC system using an interactive program enabled LFC generation in approximately 5 min, excluding warm-up time. The observations using the IRD instrument over 4 years have proven that our LFC system is practical and stable. The LFC system operated stably without major problems during this period, helping to maintain a high radial velocity accuracy.

Keywords: astro-comb; radial velocity; laser frequency comb

Paper 23142G received Nov. 30, 2023; revised Apr. 5, 2024; accepted Apr. 26, 2024; published May 14, 2024.

1 Introduction

Since Mayor and Queloz first demonstrated the existence of exoplanets using the radial velocity (RV) method in 1995,[1] more than 5500 exoplanets have been discovered through various observations, including RV and space telescope transit methods. The high accuracy radial velocity planet searcher (HARPS) has not only discovered more than 250 exoplanets, including Earth-like planets,[2,3] but has also focused on laser frequency comb (LFC) technology, leading to the early realization of a visible-wavelength astro-comb.[4–6] LFC can cover many wavelength bands with extremely precise mode spacing, and its practical efficacy has been demonstrated by several projects, including HARPS and fiber optics Cassegrain echelle spectrograph.

Most exoplanets discovered thus far orbit solar-type stars (FGK-type stars). M-type dwarf stars, which are more numerous near the solar system and in the Galaxy, have attracted significant attention in recent years. M-dwarfs have lower masses than solar-like stars and their

*Address all correspondence to Takuma Serizawa, serizawa@go.tuat.ac.jp

habitable zones are closer to their host stars, making it possible to detect low mass planets with relatively larger RV signals. Among them, late-M dwarfs have low temperatures (below 3200 K) and low masses (below 0.2 MSun); thus, Earth-like planets can be detected with an RV measurement precision of approximately 2 m/s. Late-M dwarfs are brighter in the near-infrared (NIR) region than in the visible region, making the NIR a priori more efficient for observations of late-type stars.

For these reasons, several observation projects have developed NIR instruments to investigate M-dwarfs. Habitable-zone planet finder has developed an NIR LFC covering the 810 to 1280 nm wavelength range and aims to discover M dwarfs through wavelength calibration using an astro-comb.[7,8] Calar Alto high-Resolution search for M dwarfs with Exoearths with NIR and optical echelle spectrographs (CARMENES), which uses two spectrographs attached to the 3.5 m telescope covering the visible and NIR spectral regions, has an extremely wide band (520 to 1710 nm).[9] SpectroPolarimetre InfraRouge (SPIRou) also covers a wide spectral range of 980 to 2350 nm in the NIR region.[10] Both CARMENES and SPIRou are distinctive in that they implement a Fabry–Perot (FP) etalon comb (consisting of a hollow cathode lamp and an FP) as a wavelength calibrator.[11,12] They achieve an RV precision of around 2 m/s from on-sky observations of RV standard stars, demonstrating that the FP comb has comparable performance to the LFC.[13,14] Consequently, the FP comb, as well as the LFC is recognized as an essential component for the discovery of Earth-like exoplanets.

An NIR RV survey focusing on late-M dwarfs called the infrared Doppler (IRD) project started in February 2019 within the framework of the Subaru Strategic Plan.[15] The goal of this project is to reveal the planet distribution beyond the snow line and discover Earth-like exoplanets in habitable zone using a high-resolution NIR spectrometer and an LFC system as a wavelength reference. To cover the deep absorption lines of late-M dwarfs, the LFC system provides an extremely broadband NIR spectrum from 970 to 1750 nm with a wide mode spacing of 12.5 GHz. Over the past 4 years, more than 130 nights of observations have been made using the LFC system. Despite the lack of direct maintenance for two and a half years due to Covid-19, the system continued to operate without any interruption to the observations and contributed to maintaining long-term instrument stability of about 2 m/s. Our LFC system at the 4200 m Mauna Kea summit has demonstrated significant advantages, including robust operation, high uptime, and easy remote control for turnkey operation. Here, we describe the current status of the LFC system in the IRD instrument.

2 Infrared Doppler Instrument on Subaru Telescope

Figure 1 shows a schematic of the IRD instrument. The LFC emitted from the astro-comb system, which consists of a comb generator and an optical processor, is split into a single-mode fiber (SMF) and a multi-mode fiber (MMF). In general, starlight captured with the Subaru Telescope is

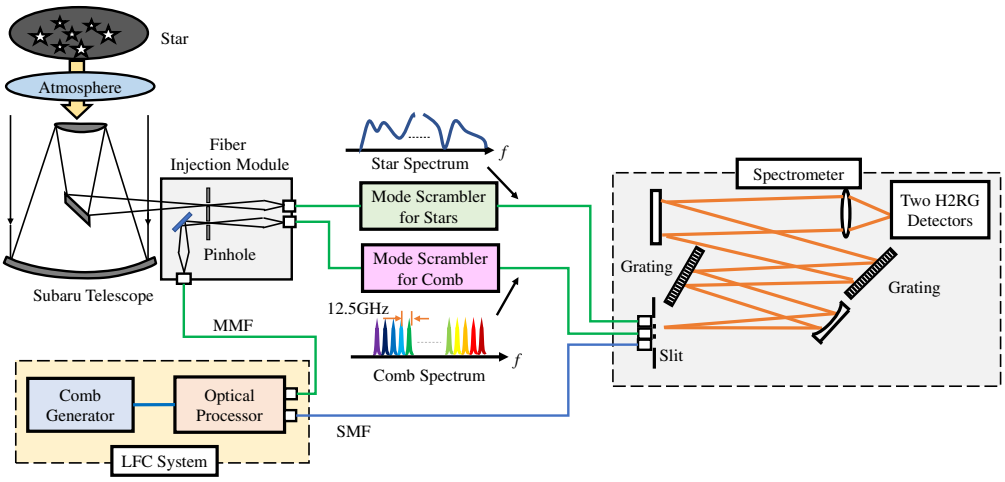

Fig. 1 A schematic of the IRD instrument on the Subaru Telescope. Blue and green lines show SMFs and MMFs, respectively.

faint, so it is introduced into the spectrometer using the MMF to maximize captured light. The near-field pattern (NFP) at the output end of the MMF tends to fluctuate because of the stress applied to the fiber. To make the NFP uniform, dynamic mode scramblers (MS), which periodically twist or bend the MMF, were installed in front of the spectrometer.

The light fed into a high-resolution ($R = 70{,}000$) cross-dispersed echelle spectrometer covering 970 to 1750 nm was spatially dispersed at each wavelength using a two-stage diffraction grating. Star and comb spectra were arranged in parallel and developed two-dimensionally on the detection surfaces of two H2RG (HAWAII-2RG) detectors. A spectrographic image of the YJ band was taken by one detector and that of the H band was taken by the other. To avoid the effects of air fluctuations, the spectrometer was placed in a vacuum chamber and was cooled to ~180 K (optics) and 79 K (detectors) to reduce thermal-background and dark-noise.[16] Our IRD astro-comb has a wide bandwidth in the NIR region, covering wavelengths ranging from 970 to 1750 nm. It has a mode spacing of 12.5 GHz and a frequency stability of 0.04 m/s (details in Sec. 6), which is accurate enough to detect Earth-like planets around M dwarfs. Figure 2 shows the combined two-dimensional echelle spectrum of the star and comb recorded on two H2RG detectors. The YJ band detector covers the wavelength range from 970 to 1366 nm and the H band detector covers the wavelength range from 1420 to 1760 nm, respectively. The IRD comb provides a reference wavelength with a frequency spacing of 12.5 GHz, as shown in the inset enlarged around 1280 nm.

The Subaru Telescope is located in an environment with a temperature range of 1°C to 5°C and an atmospheric pressure of 0.6 atm. Observations are carried out all night, so the LFC system must start easily with a turnkey operation. As shown in Fig. 3(a), the LFC generator and optical processor, which were previously installed in the barracks set, were mounted on a 19-inch rack.[17] Additionally, to ensure a thermostatic environment, the system was placed in a constant-temperature room (25 ± 0.5°C) as shown in Fig. 3(b). Moreover, all devices required for LFC generation and processing (including optical spectrum analyzers (OSAs) and other measuring instruments) were remotely controlled from a PC. This remote control could generate an LFC in approximately 5 min, excluding warm-up time. In the NIR region where there are many water vapor absorption lines, there exist several atmospheric windows with relatively few absorption lines. These atmospheric windows are affected by atmospheric and meteorological conditions at the time of observation, resulting in fluctuations in the telluric lines and lower RV accuracy. To address this issue, a data analysis pipeline was developed and applied to the RV analysis using the IRD instrument.[18] The absolute wavelength calibration on the detectors is ensured by comparing the LFC spectral lines with Th-Ar lines for each IRD observing run. We found a total RV error of 3 m/s over 700 days of on-sky monitoring observations of an RV standard star, GJ 699, which yields an instrument-derived error of about 2 m/s (Kotani et al.

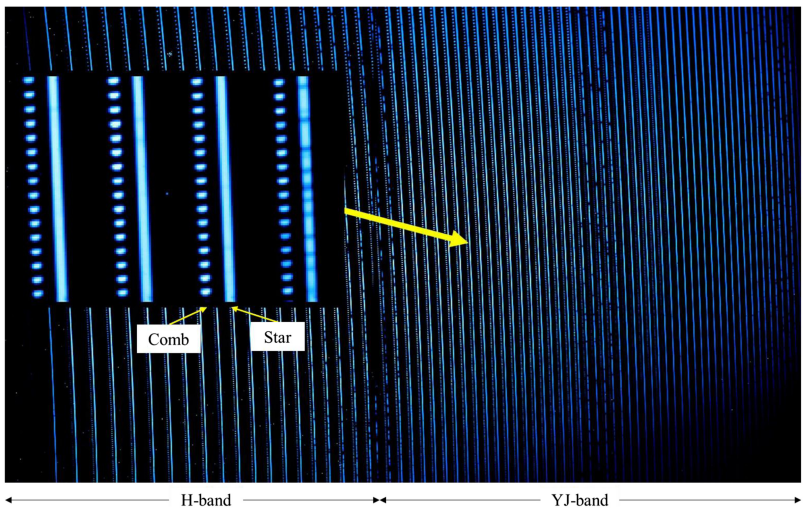

Fig. 2 The combined two-dimensional echelle spectrum of the star and comb recorded on two H2RG detectors. The comb provides a reference wavelength with a frequency spacing of 12.5 GHz, as shown in the inset enlarged image.

(a) (b)

Fig. 3 (a) LFC system mounted in 19-inch racks and (b) constant-temperature room containing LFC system.

in prep.). As a result of 4 years of observations using the IRD instrument, a super-Earth was successfully discovered near the habitable zone of a late M-type star (Ross 508b) in 2022,[19] as recently reported.

3 LFC Generation Through Pulse Shaping

Broadband LFC spectrum can be generated with high peak power pulses, which are typically available only at repetition rates of 10 MHz or less. However, an astro-comb requires conflicting characteristics, such as a broad bandwidth exceeding several hundred nanometers and a wide mode spacing of more than 10 GHz. Therefore, we employed an electro-optic modulator based LFC generation method, which is one of several astro-comb architectures.[20]

A schematic of the proposed comb generation method using pulse shaping[21] is shown in Fig. 4. First, a seed comb consisting of several 10 sidebands with 12.5 GHz frequency spacing was produced by phase-modulation of continuous-wave light emitted from a frequency-stabilized laser diode (FSLD). The seed comb was input into an optical pulse synthesizer,[22] which formed 3-ps-wide transform-limited Gaussian pulses with a repetition rate of 12.5 GHz. The average pump pulse power was amplified to approximately 5 W by a high-power erbium-doped fiber amplifier. After amplification, we eliminated the amplified-spontaneous-emission noise of the pump pulse using an FP filter (FPF) with a finesse of ~200. The moderately high finesse of 200 was sufficient to suppress noise though we did not use it for mode filtering. After passing through an FPF, the pulses were compressed using an optical pulse compressor (OPC) to enhance

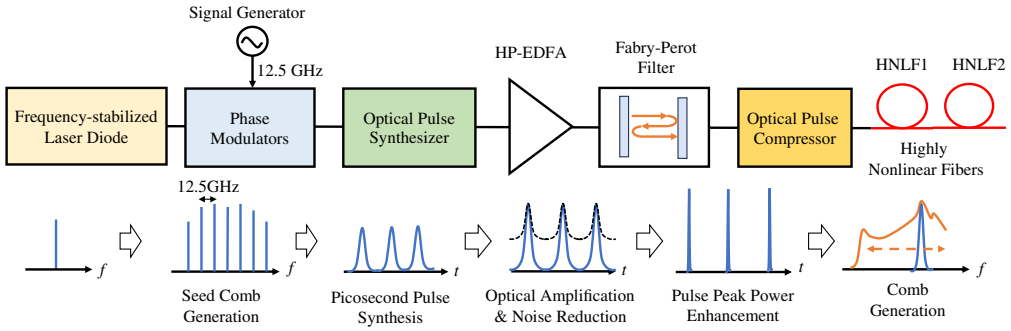

Fig. 4 A schematic of comb generation using pulse shaping.

the peak power. Finally, the pulses were launched into two cascaded highly nonlinear fibers (HNLFs) with zero-dispersion wavelengths in the 1300 to 1430 nm range to generate a broadband comb.

The comb bandwidth used at the beginning of the observations in 2019 was limited to 1050 nm at the short-wavelength edge.[21] Recently, the pulse peak power was increased from 700 to 2500 W by employing an OPC with a high compression rate. Consequently, the comb bandwidth was extended to 950 to 1750 nm, which completely covered the spectrometer bandwidth.[23] Owing to the large number of late-M dwarf absorption lines, especially in the 970 to 1050 nm range, the RV measurement precision is expected to improve by approximately 20%.

4 Optical Processing for Comb Light

Starlight is incoherent, unpolarized, and extremely faint. In contrast, LFC uses laser light, so it has high coherence and polarization. Therefore, several optical processes are required before the light is fed into the spectrometer. Figure 5 shows the configuration of the developed optical processor. The power spectral density of the comb light produced from HNLFs was approximately 3×10^{-3} W/nm. In contrast, that of the starlight emitted to the detectors in the spectrometer was on the order of 10^{-15} to 10^{-16} W/nm. Thus, the power of the comb light must be reduced by 12 to 13 orders of magnitude while maintaining its broad spectral bandwidth. Owing to the extremely wide wavelength bandwidth, we initially considered a free-space optics configuration with optical elements placed on an optical bench. However, the free-space optics configuration has long-term stability issues; therefore, we developed an inline fiber module with optical elements placed between fiber collimators (Fig. 6). By coupling the fiber modules with optical connectors, an arbitrary optical configuration with long-term stability was realized.

Next, a programmable wavelength filter (PWF) employing a liquid-crystal spatial modulator was used to flatten the comb spectrum. The PWF output spectrum was monitored using an OSA, and the comb spectrum was flattened by adjusting the attenuation of the PWF every 2 nm. Changes in the comb spectrum during the spectral shaping process were measured using an OSA with a resolution of 1 nm (Fig. 7). The uniformity of the spectrum intensity was improved within 20 dB after passing through the fixed filters and PWF.

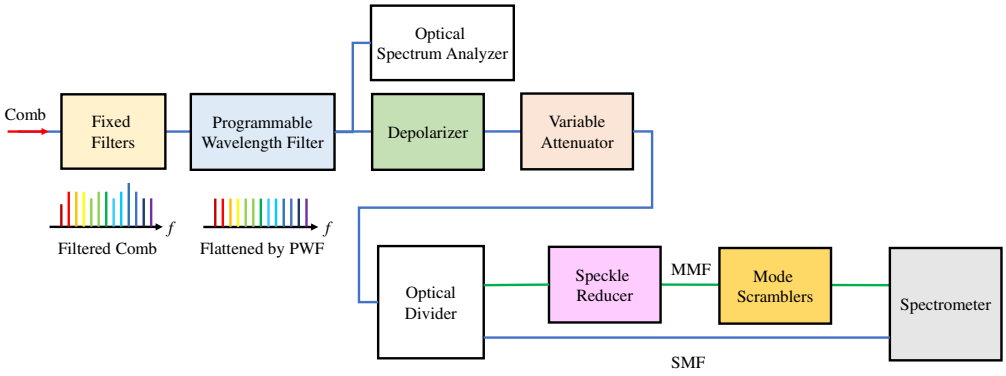

Fig. 5 Optical processor configuration for LFC.

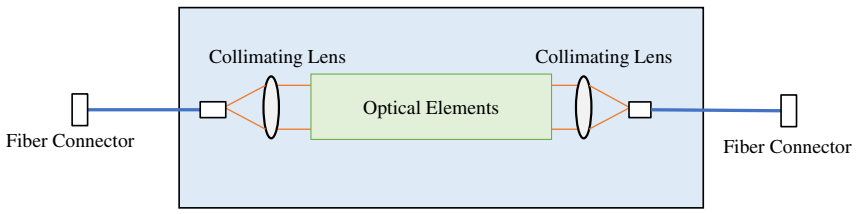

Fig. 6 In-line fiber module with optical elements placed between fiber collimators.

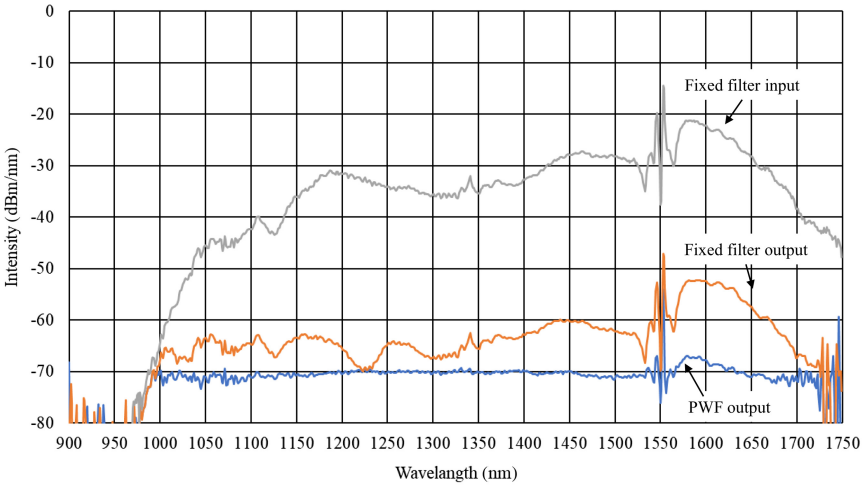

Fig. 7 Comb spectra measured using an OSA. The gray, orange, and blue lines show the comb spectrum before passing through fixed filters, after passing through fixed filters, and after being flattened by the PWF, respectively.

After flattening the spectrum, the comb light was input to a depolarizer because the diffraction grating of the spectrometer has polarization-dependent characteristics. Half- and quarter-wavelength plates were placed between two fiber collimators and rotated independently at different speeds (HWP: 180 rpm, QWP: 80 rpm). Depolarization was performed in a shorter time (approximately 1 min) than the exposure time of the detector. Subsequently, a variable optical attenuator with a rotating neutral density filter was used to adjust the attenuation level between 0 and 30 dB depending on the brightness of the starlight. After passing through the attenuator, the comb light was split into the SMF and MMF. In general, the MMF was used to carry starlight from the telescope focal plane to the spectrometer, so the comb light split into the MMF passed through a speckle reducer (SR) and MS, and finally into the spectrometer. The power of the comb light was attenuated by approximately 44 dB by the SR and MS.

Figure 8 shows the spectra of the comb and a late-M dwarf (GJ436) captured by two H2RG detectors in the spectrometer. The difference between the comb spectra in Figs. 7 and 8 is due to the different positions at which they were measured. The comb spectra in Fig. 7 were measured by OSA immediately after the PWF, whereas the comb spectrum in Fig. 8 was measured by the spectrometer; the spectral flatness in Fig. 8 was impaired due to some instrumental losses

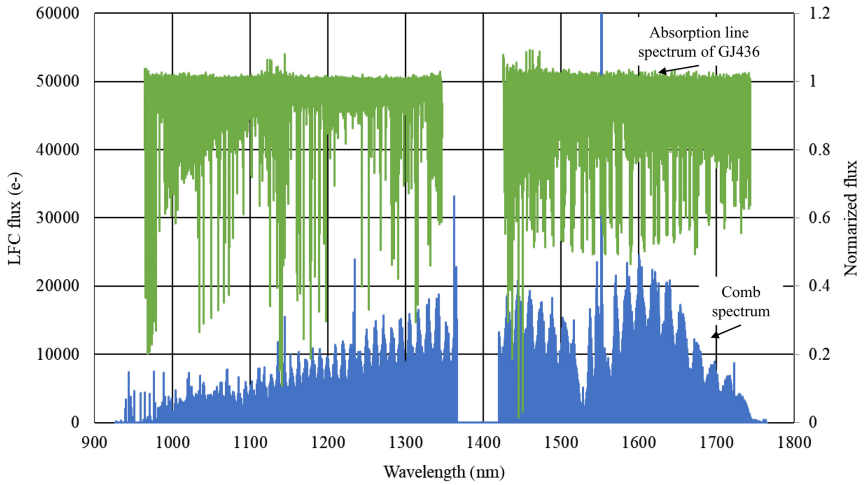

Fig. 8 Spectra of comb and a late-M dwarf captured by two H2RG detectors in the spectrometer: The blue and green lines show the comb spectrum and absorption line spectrum of GJ436, respectively. The left and right vertical axes show the photon counts for the LFC and the normalized photon counts for GJ436, respectively.

between the PWF and the spectrometer, especially at the short wavelength end. The comb spectra on the spectrometer finally covered a bandwidth range of 1000 to 1730 nm, where the GJ436 spectrum contains many absorption lines. Because late-M dwarfs have many absorption lines, especially in the wavelength region shorter than 1050 nm, the comb spectrum is expected to contribute to further improvements in accuracy.

5 Mode Scramblers for Comb Light

The final problem is modal noise affecting the comb light in the MMF. Highly coherent light, such as that of the LFC, causes speckle noise when propagating in an MMF and spectrometer, so the coherence must first be reduced as much as possible. Even with low-coherence light, when monochromatized on the camera plane, modal noise was generated owing to interference between modes in the MMF. Modal noise causes a fake RV shift and leads to RV measurement errors. To minimize modal noise, we developed an SR and two types of dynamic MS.[24]

Figures 9(a) and 9(b) show the experimental setup for evaluating the MS effects and the specific structures of the SR and MSs, respectively. The MMF used to connect them had a core diameter of 60 μm and a numerical aperture of 0.22. The SR consisted of two types of holographic diffusers (Edmund Optics, UV HOLOGRAPHIC DIFFUSER 1 and 5 DEG) placed between the collimators. These diffusers rotated at different speeds around the optical axis and reduced the coherence of the LFC light. The comb light with reduced coherence then propagated through the MMF, and two types of MS (twist and bend) made the mode pattern in the MMF uniform. MS1 (GiGa Concept, GIG-6202-200) twisted the MMF using two electric motors. MS2 consisted of a 10-m MMF with 10 loops with radii of 0.10 m and a seesaw shaker. A seesaw shaker mounted on one side of the fiber loops simultaneously moved 20 bending points. The SR and the two MSs were connected by long MMFs because the long MMFs enhanced the performance of dynamic scramblers.[24]

Figure 10 shows the experimental results of the MS for coherent light. Without the SR and two MSs, the NFP of having passed through the MMF was distorted by speckle noise, as shown in Fig. 10(a). However, the NFP obtained using the SR and MSs shown in Fig. 10(b) shows that the modal noise was sufficiently suppressed, resulting in a uniform NFP.

Next, we confirmed that the modal noise was effectively suppressed when the MMF with MSs was intentionally stressed. Figures 10(c) and 10(d) show the temporal variations of the centroid in the X and Y directions of NFP. The MMF before the SR was intentionally stressed 3 minutes later. The change in the centroid was large without MS (c), whereas with MS (d), the centroid shift was very small and recovered quickly. These experimental results showed that the developed MS effectively suppressed modal noise.

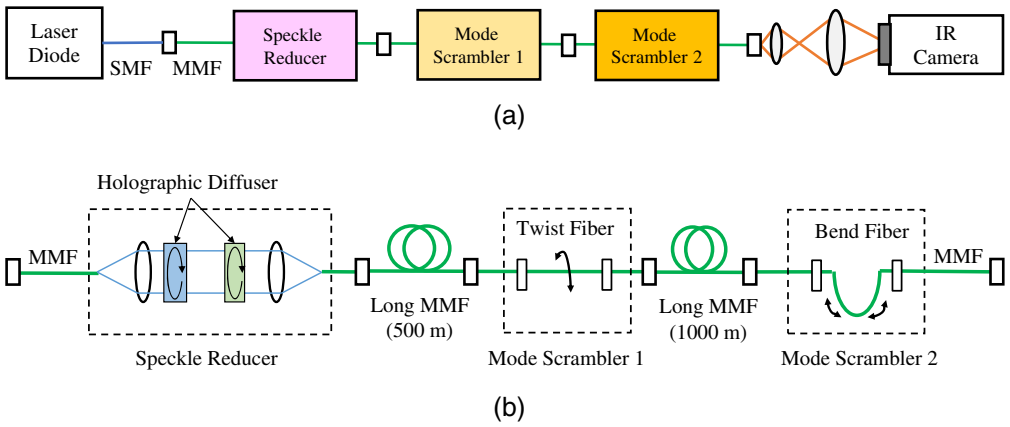

Fig. 9 (a) Experimental setup for evaluating the MS effect. LD light was injected into an SR and MS, NFP images without and with the SR and two MSs were taken with an IR camera. (b) Specific structures of the SR and two types of dynamic MS.

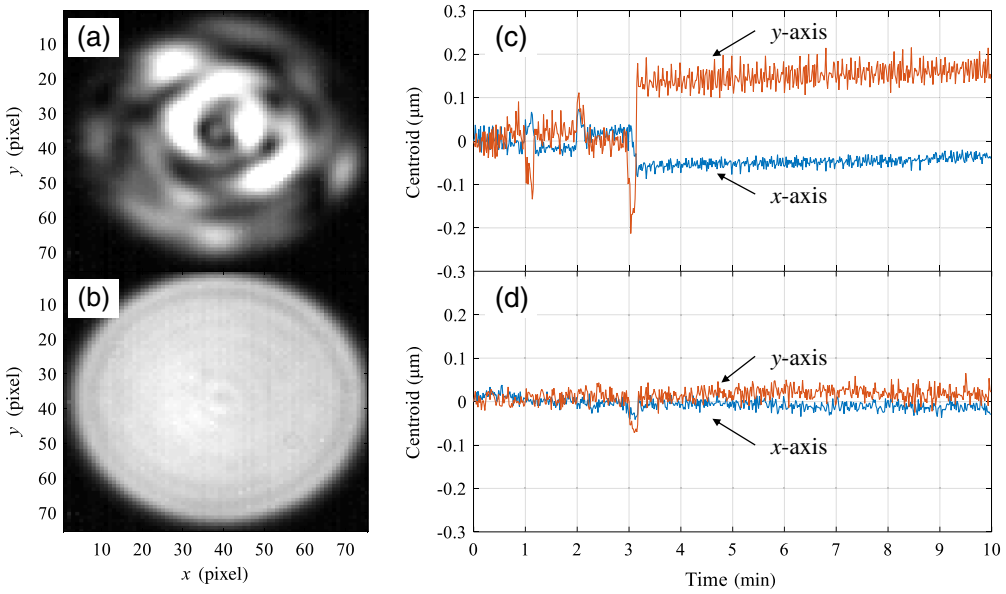

Fig. 10 NFP images (a) without and (b) with SR and MSs. Temporal changes in the centroid of the NFP in the *x*- and *y*-directions when the MMF was intentionally stressed (c) without and (b) with MS. The blue and orange lines indicate shifts of the centroid on the *x*- and *y*-axes, respectively.

6 Discussion of Frequency Stability of LFC and Instruments

High frequency accuracy is required for astro-combs to ensure high RV measurement accuracy. Additionally, the frequency stability of the instruments, including the spectrometer, should be ensured. Poor frequency stability of instruments can cause frequency fluctuations in star and comb light. In this section, we discuss the effects of the frequency stability of the comb and instruments on the precision of RV measurements.

The first factor is the frequency stability of the comb itself. This is determined by the stability of the CW laser and the accuracy of the RF oscillator, which provides the comb mode spacing. To obtain stable comb light, the IRD system employed an FSLD locked at the hydrogen cyanide absorption line (1548.955 nm). For the RF oscillator, a rubidium oscillator (10^{-11} stability at 10 s averaging time) was used as the external reference frequency to accurately define the mode spacing. A reference laser with high-frequency stability is required to investigate the long-term frequency stability of the comb. We used an acetylene frequency-stabilized LD (ACLD; NEOARK CORPORATION) with an Allan deviation of less than 10^{-12} for averaging times between 10 and 10,000 s as the reference laser. The optical beat signal between one mode extracted from the comb and the CW light emitted from the ACLD was measured for approximately 6 days.[25] The measurement system was set up in a constant-temperature room (26 ± 1°C). Figure 11(a) shows the temporal variation in the beat frequency. The frequency deviation obtained during the entire measurement was 0.03 MHz. The Allan deviation of the comb calculated from the above result was on the order of 10^{-11} for averaging times ranging from 10 to 10,000 s, as shown in Fig. 11(b). The frequency deviation of 0.03 MHz was the same across the entire comb spectrum, yielding an average value of 0.04 m/s for the corresponding RV precision.

Next, we discuss the frequency stability of the instruments. Figure 12(a) shows the experimental setup used to verify the frequency stability of the instruments. Comb light split into two SMFs (approximately 50 m) and one MMF with MS configuration in Fig. 9(b) (approximately 1.5 km) entered the spectrometer. Their comb spectra were captured by two H2RG detectors set with an exposure time of 180 s, and the measurements were performed at intensity levels where photon noise was negligible. Figures 12(b) and 12(c) show enlarged output images from the optical fibers. The frequency change was obtained from the position change in the output images. As the MMF has a larger numerical aperture than the SMF, the output image from the MMF is considerably larger than that from the SMF.

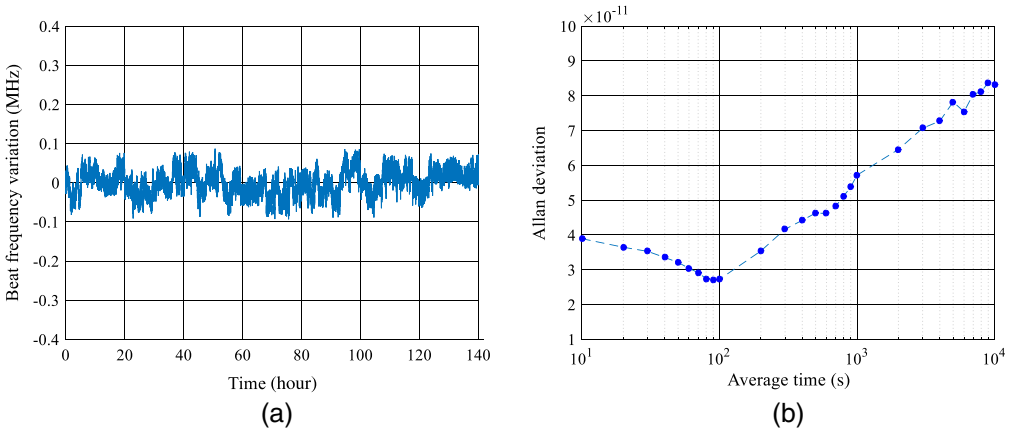

Fig. 11 Measured frequency stability of the comb: (a) temporal variation of optical beat frequency between one mode extracted from the comb and the CW light emitted from the ACLD. (b) Allan deviation calculated from the temporal variation for averaging times between 10 and 10,000 s.

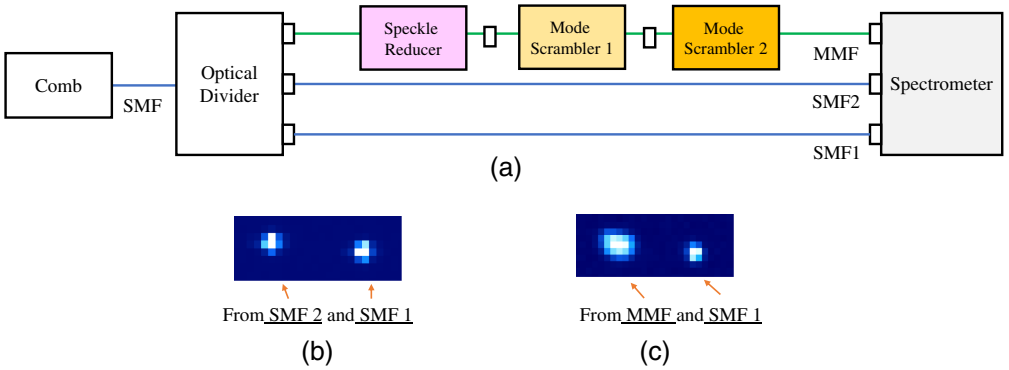

Fig. 12 (a) Experimental setup to verify the frequency stability of the instruments. Comb light split into two SMFs and one MMF entered the spectrometer, and the comb spectra were captured by two H2RG detectors. All MS were placed near the spectrometer. (b) Enlarged output images from two SMFs and (c) enlarged output images from SMF1 and MMF.

The data reductions were performed as follows. First, the bias of each channel was subtracted for all obtained H2RG data frames. Scattered light was then subtracted from the bias-corrected images. Second, the one-dimensional (1D) spectra were extracted from the 2D-spectral images. 1D spectra were obtained separately for SMF1, SMF2, and MMF with reference to black body lamp spectra. Figure 13(a) shows two examples of 1D spectra that were obtained using the SMF1 and MMF for a specific order. These spectral lines were extracted around 1449 to 1468 nm. Figure 13(b) indicates the enlarged results after Gaussian fitting around the central part of Fig. 13(a). The third step was to identify the peak position of the LFC line on the detector from the Gaussian profile results. When converting the peak position from pixel to frequency, we assumed that they were precisely aligned every 12.5 GHz in the frequency domain. Finally, for all the MMF or SMF spectra, we calculated their cross correlation functions (CCFs) between an MMF or SMF frequency-based spectra so that their velocity drifts were derived. The frequency drift at a given point in time was determined by calculating a weighted average based on the frequency fluctuations obtained from each comb light.

The absolute frequency drifts of the SMF1 and SMF2 comb spectra are shown in Fig. 14(a). The frequency drift was obtained by weighted averaging approximately 10,000 measured comb lines. The absolute frequency drifts of both SMF comb spectra showed a large systematic change during the observation period (approximately 3 days), with a peak-to-valley variation of approximately 49 MHz. This systematic frequency drift was inferred to be caused by a slight temperature change in the camera lens of the spectrometer. Figure 14(b) shows the relative frequency

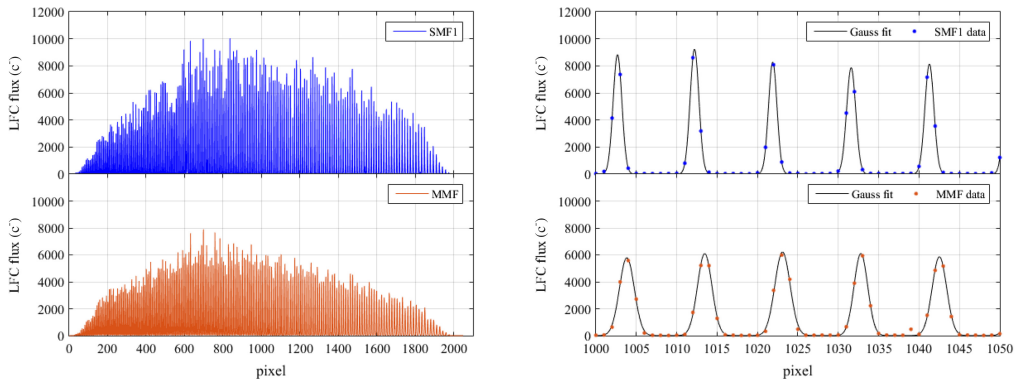

Fig. 13 Examples of LFC spectra obtained from SMF1and MMF1. (a) Two LFC spectra obtained after tracing the echelle order. (b) Gaussian fit results for a portion of the two spectra shown in panel (a).

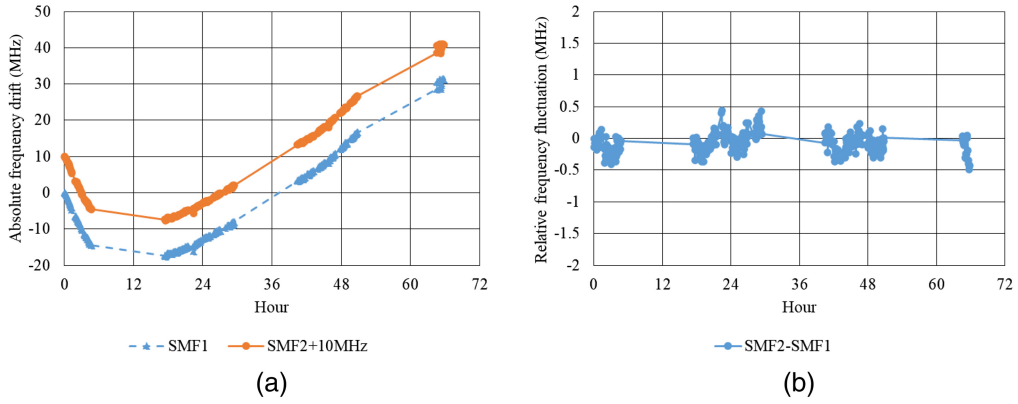

Fig. 14 (a) Absolute frequency drifts of comb spectra observed with two SMFs. Artificial offsets of 10 MHz were added to the original frequency measurements of SMF2's spectra for display purposes. (b) Relative frequency fluctuation between the two SMF comb spectra.

fluctuation, which is the simple difference between the absolute drifts of the two SMFs. The resulting relative fluctuation did not vary systematically and had a small deviation of 0.15 MHz, which corresponds to an RV precision of 0.23 m/s. This slight error could have been caused by polarization-induced error due to insufficient depolarizer capacity and/or slight inhomogeneities in the detector pixels.

The absolute frequency drifts of the SMF1 and MMF comb spectra showed different systematic changes from each other during the observation period (about 1 week). Each frequency drift was determined by a weighted average of about 10,000 measured comb lines. The peak-to-valley variation was approximately 40 MHz for SMF1 and approximately 34 MHz for MMF, as shown in Fig. 15(a). The difference in absolute frequency drift between SMF1 and MMF is due to the considerable difference in the size of the output images from SMF1 and MMF. In order to remove systematic errors due to the difference in size of the SMF1 and MMF output images, we performed a correction using a regression line in which a linear function was applied to the relationship between the absolute drifts of MMF and SMF1. Figure 15(b) shows the relative frequency fluctuation between SMF1 and MMF obtained after CCFs. The frequency fluctuation is as small as 0.30 MHz, corresponding to an RV precision of 0.46 m/s, which is 0.23 m/s larger than that for the two SMFs. Modal noise did not occur in the SMF but only in the MMF. Therefore, this small increase of 0.23 m/s is estimated to be mainly due to modal noise, indicating that the modal noise was effectively suppressed by the MS.

RV errors measured using LFC in laboratory tests were 0.23 m/s between SMF1 and SMF2 and 0.46 m/s between SMF1 and MMF, respectively. These values are very small compared to

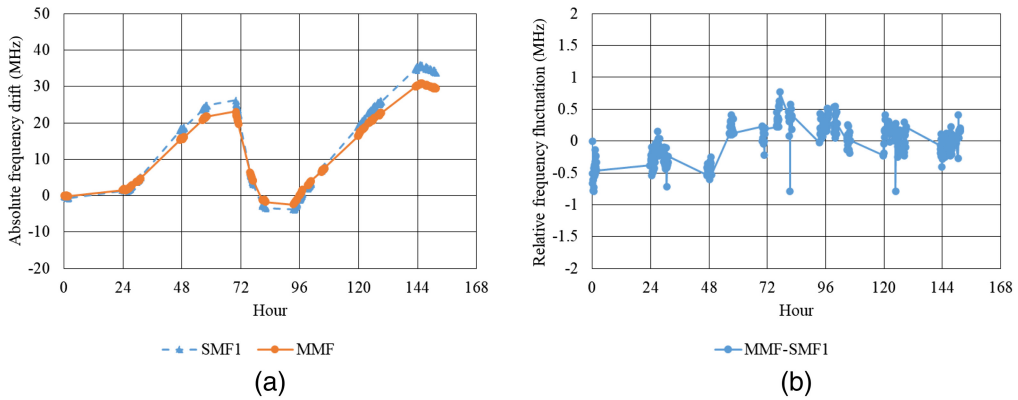

Fig. 15 (a) Absolute frequency drifts of comb spectra observed with SMF1 and MMF comb. (b) Relative frequency fluctuation between SMF1 and MMF comb spectra.

instrument-derived errors of about 2 m/s obtained from long-term observations of RV standard stars. We found that the RV drift of the spectrograph is strongly correlated with temperature variations of the camera lens just in front of the detectors. Improvement of the temperature stability of the spectrograph is expected to reduce the instrument-derived error (Kotani et al. in preparation).

Finally, we would like to add a few words regarding the data reduction method used to obtain the frequency variation. Because the LFC repetition frequency of 12.5 GHz is very precise, we analyzed the comb images on the camera by assuming that they were aligned every 12.5 GHz. Thus, the entire analysis process can be performed at the optical frequency without the need for spectral referencing of Th-Ar lamps or conversion to absolute wavelengths.

7 Conclusions

An LFC system with a broadband spectrum ranging from 970 to 1750 nm was developed for extensive surveys of mid-to-late M-type dwarfs. Owing to the simple and robust LFC generation method, the generated LFC light has a frequency stability of 0.03 MHz, corresponding to 0.04 m/s in RV. This is two orders of magnitude more stable than the target RV measurement precision of 2 m/s. The LFC system also employed an in-line fiber module to enable any optical system configuration for the optical processor. This fiber-optic configuration allows for long-term stability and easy repair. Moreover, simple remote control of the LFC system using an interactive program enabled LFC generation in approximately 5 min, excluding warm-up time.

The frequency stability of the instruments was investigated using the LFC. The resulting frequency stability had a standard deviation of 0.30 MHz, which corresponded to an RV of 0.46 m/s.

Observations using the IRD instrument over four years have proven that our LFC system is practical and stable. In 2022, it was reported that a super-Earth was successfully discovered near the habitable zone of a late M-type star (Ross 508b).[19]

Disclosures

The authors declare that there are no conflicts of interest.

Code and Data Availability

The data presented in this article is not publicly available. If you require these data, you can request them from the corresponding author at the email address above.

Acknowledgments

The research presented in this article includes a report published in Proceeding of SPIE 12188, Advances in Optical and Mechanical Technologies for Telescopes and Instrumentation V,

121885J (29 August 2022). M.T. was supported by JSPS KAKENHI (Grant Nos. 18H05442, 15H02063, and 22000005).

References

1. M. Mayor and D. Queloz, "A Jupiter-mass companion to a solar-type star," *Nature* **378**, 355–359 (1995).
2. X. Bonfils et al., "A temperate exo-Earth around a quiet M dwarf at 3.4 parsec," *Astron. Astrophys.* **613**, A25 (2018).
3. M. Mayor et al., "Setting new standards with HARPS," *The Messenger* **114**, 20–24 (2003).
4. T. Wilken et al., "A spectrograph for exoplanet observations calibrated at the centimetre-per-second level," *Nature* **485**, 611–614 (2012).
5. R. A. Probst et al., "Relative stability of two laser frequency combs for routine operation on HARPS and FOCES," *Proc. SPIE* **9908**, 990864 (2016).
6. R. A. Probst et al., "A crucial test for astronomical spectrograph calibration with frequency combs," *Nat. Astron.* **4**, 603–608 (2020).
7. A. J. Metcalf et al., "Stellar Spectroscopy in the near-infrared with a laser frequency comb," *Optica* **6**(2), 233–239 (2019).
8. S. Kanodia et al., "Overview of the spectrometer optical fiber feed for the habitable-zone planet finder," *Proc. SPIE* **10702**, 107026Q (2018).
9. A. Quirrenbach et al., "CARMENES: high-resolution spectra and precise radial velocities in the red and infrared," *Proc. SPIE* **10702**, 107020W (2018).
10. "SPIRou (SPectropolarimètre InfraROUge) Near-infrared spectropolarimeter with high radial-velocity precision," https://www.cfht.hawaii.edu/Instruments/SPIRou/index.php.
11. T. Trifonov et al., "The CARMENES search for exoplanets around M dwarfs. First visual-channel radial-velocity measurements and orbital parameter updates of seven M-dwarf planetary systems," *Astron. Astrophys.* **609**, A117 (2018).
12. M. J. Hobson et al., "The SPIRou wavelength calibration for precise radial velocities in the near infrared," *Astron. Astrophys.* **648**, A48 (2021).
13. I. Ribas et al., "The CARMENES search for exoplanets around M dwarfs," *Astron. Astrophys.* **670**, A139 (2023).
14. J.-F. Donati et al., "SPIRou: NIR velocimetry and spectropolarimetry at the CFHT," *Mon. Not. R. Astron. Soc*, **498**(4), 5684–5703 (2020).
15. "IRD project," https://ird.mtk.nao.ac.jp/IRDpub/index_tmp.html.
16. T. Kotani et al., "The infrared Doppler (IRD) instrument for the Subaru telescope:instrument description and commissioning results," *Proc. SPIE* **10702**, 1070211 (2018).
17. T. Kokubo et al., "12.5-GHz-spaced laser frequency comb covering Y, J, and H bands for Infrared Doppler instrument," *Proc. SPIE* **9912**, 99121R (2016).
18. T. Hirano et al., "Precision radial velocity measurements by the forward-modeling technique in the near-infrared," *Publ. Astron. Soc. Jpn.* **72**(6), 93 (2020).
19. H. Harakawa et al., "A super-Earth orbiting near the inner edge of the habitable zone around the M4.5-dwarf Ross 508," *Publ. Astron. Soc. Jpn.* **74**(4), 904–922 (2022).
20. R. A. Mccracken et al., "A decade of astrocombs: recent advances in frequency combs for astronomy," *Opt. Exp.* **25** (13), 15058–15078 (2017).
21. K. Kashiwagi et al., "Direct generation of 12.5-GHz-spaced optical frequency comb with ultrabroad coverage in near-infrared region by cascaded fiber configuration," *Opt. Exp.* **24**(8), 8120–8131 (2016).
22. H. Tsuda et al., "Analog and digital optical pulse synthesizers using arrayed-waveguide gratings for high-speed optical signal processing," *J. Lightwave Technol.* **26**(6), 670–677 (2008).
23. T. Serizawa et al., *Bandwidth Expansion of 12.5-GHz-Spaced Laser Frequency Comb in Near-Infrared Region by Improving Pulse Compression Magnification*, pp. 1–2, IPC, Vancouver, British Columbia (2021).
24. M. Ishizuka et al., "Fiber mode scrambler for the Subaru Infrared Doppler Instrument (IRD)," *Publ. Astron. Soc. Pac.* **130**(988), 065003 (2018).
25. T. Mori et al., *12.5-GHz-Spaced Laser Frequency Comb Coveringover 100 THz and Frequency Shift of All Individual Lines for Calibration of Infrared Doppler Instrument*, pp. 156–157, IPC, Waikoloa, Hawaii (2016).

Takuma Serizawa is a postdoctoral researcher at the Tokyo University of Agriculture and Technology. He received his BS degree in engineering from Niigata University in 2012 and his MS and PhD degrees in engineering from the Graduate School of Science and Technology, Niigata University in 2014 and 2017, respectively. His current research interests include optical metrology, interferometer, and optical frequency comb systems. He is a member of SPIE.

Takashi Kurokawa joined Nippon Telegraph and Telephone Laboratories in 1973. He received his PhD in basic physics from the University of Tokyo, in 1981. Since 1998, he has been a professor of Tokyo University of Agriculture and Technology. He was engaged in the development of astro-comb systems at the National Astronomical Observatory of Japan and Astrobiology Center from 2013 to 2023. He is a fellow of the Japan Society of Applied Physics.

Yosuke Tanaka is a professor at Tokyo University of Agriculture and Technology, Japan. He received his BE degree in electronic engineering and the ME and Dr. Eng degrees in electrical engineering, all from the University of Tokyo, Tokyo, Japan, in 1991, 1993, and 1996, respectively. His research interests cover many areas of fiber optic sensing systems and the related technologies, including optical frequency comb systems and their applications.

Motohide Tamura belongs to the University of Tokyo and is cross-appointed to the director of the Astrobiology Center of National Institute of Natural Sciences. Based on his nearly 40 years of experience of infrared astronomy, he has led the astronomical observations of exoplanets and disks using the direct imaging techniques on the 8.2-m Subaru telescope (SEEDS project). He has led many infrared instrumentation projects including CIAO, HiCIAO, IRD for Subaru, and SIRIUS, SIRPOL for IRSF.

Biographies of the other authors are not available.